The optimal reflectance for a PEDOT:PSS-ITO hybrid Transparent Conducting film

Alan Chirong Li

Author Background: Alan Li grew up in China and currently attends Harrow International School Hong Kong in Hong Kong SAR, China. His Pioneer seminar topic was in the field of sciences and is titled "Material Science."

Abstract

In order to determine the optimal reflectance of a PEDOT:PSS-ITO hybrid, the refractive index and the extinction coefficient of the two materials have to be determined. A computer simulation is used to determine the optical properties, including reflectance, transmittance, and absorption, of a single stack of PEDOT:PSS-ITO hybrid under different incident ray wavelengths. The result suggests that the absorption is correlated to the ratio between the thickness of the PEDOT:PSS and ITO, which can be explained by the two materials' extinction coefficients. Moreover, the ratio of thicknesses of the two layers will then be determined to investigate the stack dependence of the reflectance. The reflectance increases as the stack number increases and decreases as the incident ray wavelength decreases. The nature of the hybrid TCF makes it useful as the DBR mirrors in a Vertical-Cavity Surface-Emitting Laser (VCSEL).

Introduction

History

Transparent conductive films (TCFs) are thin, optically transparent materials that conduct electricity. TCFs are integral components in many different fields of technology. In the past few decades, many new types of TCFs have appeared, such as carbon nanotubes (CNTs), conductive polymers, ultra-thin metal films, and many more, some with performance even better than their formerly monopolistic counterpart, transparent conducting oxides (TCOs). TCOs have been heavily utilized in many fields for over five decades[1], and numerous new

types of TCOs have been discovered in recent years. With an increasing demand for better performing TCOs, different kinds of TCOs are being tested and used in various fields according to their performance. Those fields include portable electronics, solar cells, displays, and multipurpose windows[3]. One of the earliest discoveries of TCOs dates back to as early as 1907, when cadmium oxide was made into a transparent conducting film by Karl Baedeker[6].

In recent years, the field of TCFs has widened markedly as more and more researchers join and work on different branches. The rapid development of photovoltaic devices and the ubiquity of Flat Panel Displays signal the success of TCFs, especially TCOs. In the 21st century, as global warming and environmental changes become more evident to the people who did not previously believe in climate change, the market started leaning towards sustainability, which eventually led to the flourishing of the "green technology" industries. Thus, sustainability, energy efficiency, and environmental friendliness became the new value propositions that tech companies strive to accomplish [3].

Motivation

In the 21st century, as environmental consciousness became more valued, the market sizes for industries like photovoltaic cells and low emissivity glass rose considerably. TCOs are essential parts of photovoltaic cells, and many photovoltaic cell producing companies use high performing TCOs in their products for better efficiency. The majority of the market started seeking new materials to improve the silicon photovoltaic cells. In 2007, the photovoltaic market was growing at around 50% annually; 10 years later, in 2017, the market had a growth rate of 30%[5]. These data demonstrate the vast potential PV markets have, let alone other more mature markets, such as the Flat Panel Display (FPD) market.

TCFs are favored in the FPD market mainly for their transparent and electrically conductive characteristics. The FPD market size has been growing steadily over the past several years, having a stable increase annually with no signs of slowing. In 2018, the market size was 116.8 billion dollars. All evidence suggests that TCOs can be useful in many ways to researchers and scientists.

The current state of TCFs

Currently, TCOs are the most widely used TCF materials. TCOs should have a carrier density of at least $10^{20}cm^{-3}$ to ensure electrical conductivity. This value is typically within the range of semiconductors, as a band gap is also required for TCOs to be transparent, meaning that the band gap has to be wide enough so that visible lights will not be absorbed.

The most used materials in the TCO industry include Indium Tin Oxide (InSnO), Tin Oxide (SnO_2), Indium Oxide (In_2O_3), and Zinc Oxide (ZnO), all with a satisfactory carrier density and electrical conductivity. Traditionally TCOs are mainly oxides of Zn, Cd, In, Ga, and Sn mixed with different dopants[3]. These n-type TCOs are crystalline and have cation coordination of Tetrahedral, Octahedral, or Cage Framework. The differences in cation coordination, Dopant type and concentration all affect the band gap energy and the electrical conductivity.

Although ITO is one of the most popular TCOs, occupying a 97.6% TCF market share in 2010[4], the expensive yet unstable market price of Indium is still the main shortcoming of this material. Researchers started seeking for new types of unconventional TCOs that could replace ITO, C12A7($12CaO \cdot 7Al_2O_3$) is one of them[1]. This material a conductivity of around 800 S/cm[3] was obtained after a multi-step film growth, crystallization, and in-situ annealing process.

In 1995, amorphous TCOs were created through the sintering process. These materials no longer have a fixed crystallic structure, thus making them valuable in many fields, especially the photovoltaic cell industry. When using amorphous TCOs for photovoltaic cells, more light can be utilized, because light can pass through the TCO through all directions. In fact, amorphous TCO photovoltaic cells have better performance than both monocrystalline and polycrystalline TCO photovoltaic cells[3].

Apart from TCOs, there are other organic based transparent conductors that have drawn a lot of attention and interest recently. Carbon nanotubes have drawn a lot of interest recently as the material has several advantages when compared to ITO. CNTs have a better elastic

modulus (around 1-2 TPa)[7], which makes them less prone to damages under constant mechanical stress. Moreover, CNTs also have an extremely high electrical conductivity which can be up to 10^7 S/m[7]. CNTs can also be used in addition to TCOs, which opens up more possibilities for this material.[2]

Theory

In the "PhotonicsRT: Wave Propagation In Multilayer Structures" simulation[8], reflectance and transmittance are calculated from the Fresnel Equations, as the equations describe those properties of light when incident on an interface between different optical media. The fraction of the incidence power reflected from the interface is called reflectance, R. The fraction of the incident light that is refracted into the second medium is called transmittance, T. Due to the multilayered nature of this simulation, the reflectance and transmittance need to be derived from the matrix method.

The Fresnel equations are:

$$r_s = \frac{n_1 cos\theta_1 - n_2 cos\theta_2}{n_1 cos\theta_1 + n_2 cos\theta_2}$$
$$r_p = \frac{n_2 cos\theta_1 - n_1 cos\theta_2}{n_2 cos\theta_1 + n_1 cos\theta_2}$$
$$t_s = \frac{2n_1 cos\theta_1}{n_1 cos\theta_1 + n_2 cos\theta_2}$$
$$t_p = \frac{2n_1 cos\theta_1}{n_2 cos\theta_1 + n_1 cos\theta_2}$$

where n_1 and n_2 are the refractive indices of the two mediums and θ_1 and θ_2 the angle of incidence and angle of refraction, respectively. The subscript p and s indicates whether the incident ray is p-polarized or s-polarized. We consider a multiple layer structure consisting of N layers starting from zero to N-1. Let v_n be the amplitude of the wave on the *nth* side heading away from the boundary and w_n be the amplitude on the *nth* side heading backward.[10] We define:

$$\delta_n \equiv (thickness\ of\ layer\ n)\ (k_z\ for\ the\ forward-traveling\ wave\ in\ layer\ n)$$

Where k_z is the angular wave vector and δ_n characterizes the phase and potential absorption that comes from passing through layer n.

Now we get:

$$v_{n+1} = (v_n e^{i\delta_n}) t_{n,n+1} + w_{n+1}\, r_{n+1,n}$$

$$w_n e^{-i\delta_n} = w_{n+1} + t_{n+1,n} + (v_n e^{i\delta_n})r_{n,n+1}$$

The equations can be transferred to:

$$\begin{pmatrix} v_n \\ w_n \end{pmatrix} = M_n \begin{pmatrix} v_{n+1} \\ w_{n+1} \end{pmatrix}$$

For $n = 1, \ldots, N-2,$ *where*

$$M_n \equiv \begin{pmatrix} e^{-i\delta_n} & 0 \\ 0 & e^{i\delta_n} \end{pmatrix} \begin{pmatrix} 1 & r_{n,n+1} \\ r_{n,n+1} & 1 \end{pmatrix} \frac{1}{t_{n,n+1}}$$

The waves entering the structure and the waves exiting are now related by the matrix:

$$\begin{pmatrix} 1 \\ r \end{pmatrix} = \tilde{M} \begin{pmatrix} t \\ 0 \end{pmatrix}$$

Where $\tilde{M}$ is given by:

$$\tilde{M} = \frac{1}{t_{0,1}} \begin{pmatrix} 1 & r_{0,1} \\ r_{0,1} & 1 \end{pmatrix} M_1 M_2 \cdots M_{N-2}$$

r and t in terms of the four matrices $\tilde{M}$ can be written as:

$$\begin{pmatrix} 1 \\ r \end{pmatrix} = \begin{pmatrix} \tilde{M}_{00} & \tilde{M}_{01} \\ \tilde{M}_{10} & \tilde{M}_{11} \end{pmatrix} \begin{pmatrix} t \\ 0 \end{pmatrix}$$

$$t = 1/\tilde{M}_{00}, \quad r = \tilde{M}_{10}/\tilde{M}_{00}$$

Methodology:

Due to limited access to laboratories, all of the experiments on this paper were conducted on computer simulations. All of the simulations in this paper are done on nanoHUB, which is a website that provides multiple types of computer simulations. The simulation that is used for this paper is “PhotonicsRT: Wave Propagation In Multilayer Structures.” This simulation calculates the reflection, transmission, and absorption of light passing through a lamellar structure with uniform isotropic layers. Figure 1 shows the interface of the simulation. In the top left corner, the incidence polarization can be switched, the angle of incidence, as well as the begin and end wavelengths, can also be inserted. Furthermore, multiple layers of materials can be added between the superstrate and the substrate by clicking “Add Layer.” The “Num of Stacks” option allows different stack numbers to be chosen. Lastly, by clicking on “Solve,” a graph of the structure’s reflectance, transmittance, and absorption of light will be calculated and shown.[8]

The refractive index of the ITO is from a sample purchased from Delta Technologies, LTD. (CG-60IN-CUV, ITO on BK7), and the refractive index of the PEDOT:PSS is from a sample purchased from Heraeus (Clevios^{TM} P VP Al 4083)[9]. In order to establish an ideal environment for testing, the refractive indices of both the superstrate and substrate will be set to 1, which is the value of vacuum. The incident angle will be set to 0, which is perpendicular to the structure plane. For the two types of TCF that are used, the thickness ranges from 40 to 200nm. Since the refractive index changes as the wavelengths are changed, the begin and end wavelengths will be used in increments of 50nm through the visible light range. The plotted graph shows both the transmittance (T) and reflectance (R) value. When $T+R=1$, there is no energy absorption, so $absorption = 1- (T+R)$. The thickness of the TCFs will change in increments of 40nm so that the total thickness is always 200nm.

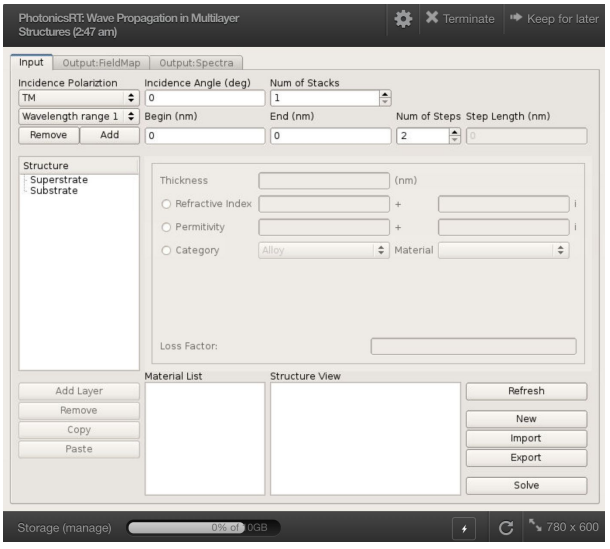

Figure 1: The interface of the simulation.

Results and Analysis

Single stack thickness dependence

Figure 2(a) and *(b)* demonstrate the refractive index n and the extinction coefficient k of the PEDOT:PSS and ITO that are used in the simulation. In *figure 2(a)*, ITO has a higher refractive index than PEDOT:PSS at all incident wavelengths. Also, the refractive index n for both materials decreases as the wavelength increases, and the relationship is almost linear between the wavelengths of 400 to 700nm. In *figure 2(b)* the extinction coefficient of PEDOT:PSS increases with an increasing gradient. The ITO has the maximum extinction coefficient at the wavelength of 400nm. The two curves intersect when the wavelength is about 480nm. All of the simulations are completed under the premise that the incident ray is always 0° and both the superstrate and the substrate are vacuums, with a refractive index of

n=1 and k=0. The values of the refractive indices of the ITOs and the PEDOT:PSS may be different from those produced by other companies with different treatments.

(a) *(b)*

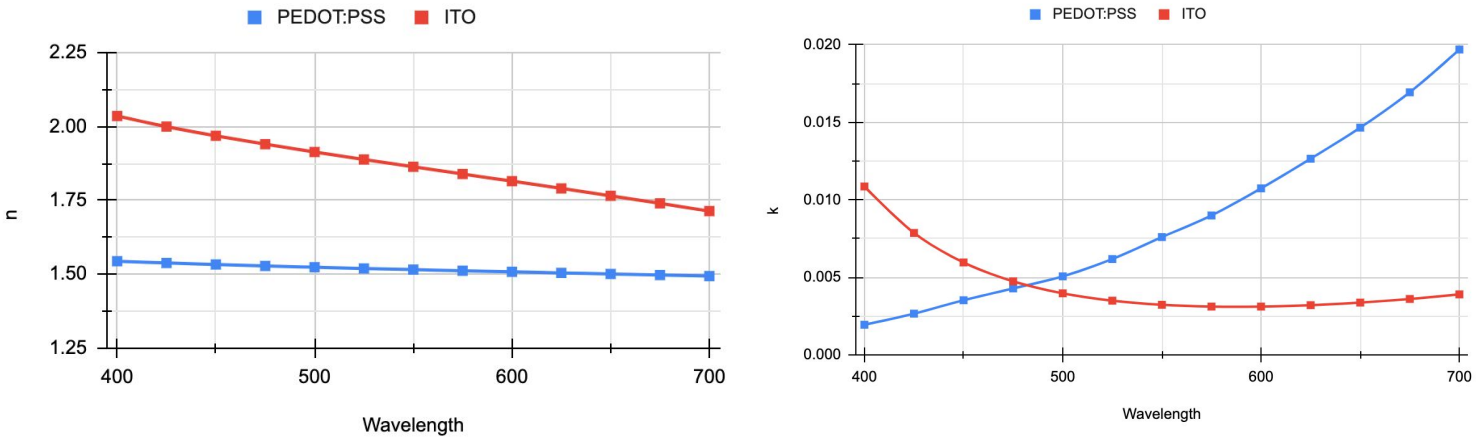

Figure 2(a)*The graph of refractive index, n, of PEDOT:PSS and ITO at different wavelengths.* ***(b)****The extinction coefficient, k, of PEDOT:PSS and ITO at different wavelengths.*

The simulation of the reflectance for different combinations of ITO and PEDOT:PSS thickness showed great variations: The maximum reflectance ranged from 0.3187 for 200nm thick ITO when the incident ray wavelength is 500nm to 0.143 for 80nm PEDOT:PSS and 120nm ITO hybrid TCF when the incident ray wavelength is at 500nm too (*figure 3(a)*).

(a) *(b)*

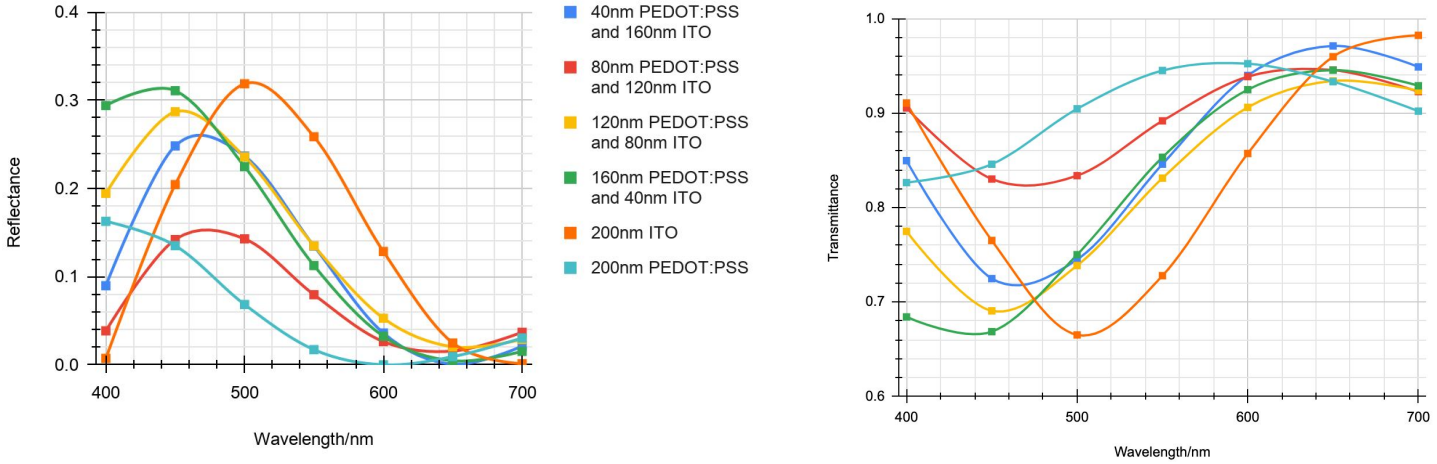

Figure 3 (a)*The graph of reflectance against wavelength for different hybrids of ITO and PEDOT:PSS TCFs, under the visible spectrum(400-700nm).* ***(b)****The graph of transmittance against wavelength for different hybrids of ITO and PEDOT:PSS TCFs, under the visible spectrum(400-700nm).*

All of the curves have a shape that vaguely resembles a sinusoidal graph, where the amplitude tends to be before the incident wavelength of 500, meaning that in the visible spectrum. The reflectance is lower when the incident ray is yellow or red, whereas the other shorter wavelength colors such as green, blue, or violet, tend to have a higher reflectance. In fact, most of the TCFs have their minimum reflectance within the visible spectrum when the incident ray wavelength is between 600 and 700nm. *Figure 3(a)* shows that 160nm PEDOT:PSS and 40nm ITO TCF has the highest reflectance when the incident ray has a wavelength between 400 and 475nm. From 475 onwards, 200nm ITO has the highest reflectance until the incident ray wavelength reaches around 660nm. Moreover, 200nm ITO has the lowest reflectance when the incident ray is from 400 to around 415nm. From 415 to around 446nm, the 80nm PEDOT:PSS and 120nm ITO have the lowest reflectance. After that, the 200nm PEDOT:PSS has the lowest reflectance until around 635nm. Overall, after 650nm, the reflectance for all TCFs start to converge; as a result, their values are all relatively close to each other.

For transmittance, *figure 3(b)* shows that the curves have values ranging from 0.9825 for 200nm ITO when the wavelength of the incident ray is at 700nm to 0.665 for 200nm ITO again when the incident ray has a wavelength of 500nm. In the graph, most of the TCF's minimum transmittance is on the left side when the wavelength is smaller than 500nm, and vice versa. Similar to the graph of reflectance, the curves are converged when the incident ray wavelength is between 600 and 700nm. The 80nm PEDOT:PSS and 120nm ITO has the highest transmittance among all of the other TCFs, from around 405 to around 440nm wavelengths, then 200nm PEDOT:PSS becomes the highest until the wavelength is around 610nm. After which the 40nm PEDOT:PSS and 160nm ITO becomes the highest until about 660nm, where 200nm ITO has the highest transmittance for the rest of the visible spectrum. 160nm PEDOT:PSS and 40nm ITO have the minimum transmittance among all of the other TCFs, from 400 to around 470nm of incident ray wavelength. 200nm ITO covers the minimum transmittance for incident rays of most of the visible spectrum, ranging up to around 630nm.

In fact, the transmittance and the reflectance can be related. When the extinction coefficient (k) is zero,

$$T + R = 1 .$$

However, when the extinction coefficient is not equal to zero, which is often the case, the transmittance and reflectance are then related by:

$$A = 1 - (T + R)$$

where A is the fraction of incident light absorbed by the material.

In *figure 4(a)*, the absorbance for different TCFs varied from 0.0818 for 200nm ITO at an incident ray wavelength of 400nm to 0.0107 for 200nm PEDOT:PSS at the same incident ray wavelength. On the graph, most of the curves intersect between the incident wavelengths of 460 and 480nm. After that range of wavelengths, until 700nm, the lines do not intersect anymore. As the PEDOT:PSS thickness decreases, the absorbance also decreases, which means that 200nm ITO has the lowest absorbance, since it does not contain any PEDOT:PSS. Moreover, the relationship between absorbance and the thickness of PEDOT:PSS is inverted when the incident wavelength is from 400 to 450nm, where the absorbance decreases as the thickness of ITO decreases. This observation could potentially be explained by *figure 2(b)*, where the extinction coefficient of the two materials intersect when the incident wavelength is about 480nm. *Figure 4(b)* shows the absorbance, reflectance, and transmittance for different TCFs at an incident wavelength of 400nm. The trend in absorbance can be observed easily from this graph as the ITO thickness changes, while the other two properties do not possess a trend that is as obvious.

(a)

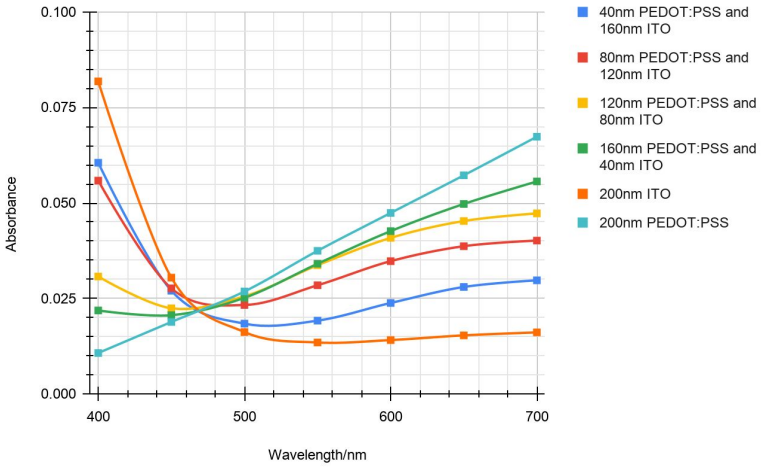

(b)

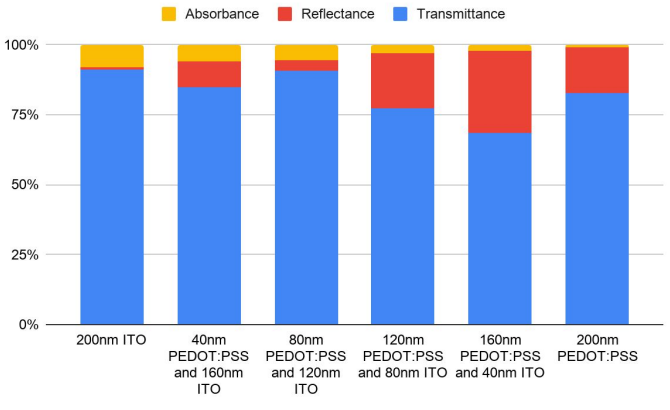

Figure 4 (a)*The graph of Absorbance against wavelength for different hybrids of ITO and PEDOT:PSS TCFs, under the visible spectrum(400-700nm).* ***(b)*** *The graph of Absorbance, reflectance, and Transmittance for different hybrids of ITO and PEDOT:PSS TCFs, under the wavelength of 400nm.*

Stack dependence for optimum thickness

In the previous section, the reflectance, transmittance, and absorbance were investigated for a single stack of hybrid TCF. Now the stack dependence of a certain combination of PEDOT:PSS and ITO will be investigated. In the *single stack thickness dependence* section, the thicknesses are all chosen randomly. In this section, the optimum thicknesses for each material under different incident ray wavelengths will be determined and used in the "PhotonicsRT: Wave Propagation In Multilayer Structures" simulation to determine the respective reflectances at different stack numbers.

Destructive interference is utilized for achieving maximum reflectance. PEDOT:PSS has a reflective index smaller than that of ITO in the visible spectrum, so both reflected waves will have a $\frac{\lambda}{2}$ shift. By using a film of thickness 25%, the incident ray wavelength results in destructive interference. The formula for the optimum thickness can be determined through a step-by-step approach[11]:

$$\Delta a = \tfrac{\lambda}{2} \qquad \Delta b = 2t + \tfrac{\lambda}{2}$$

Where Δa, Δb, and t are the shift in wavelength when the incident wave reflects off the top surface, the extra distance the ray reflecting off the bottom of the film travels, and the thickness of the film respectively. The relative shift, Δ, will then be:

$$\Delta = \Delta b - \Delta a = 2t = (m + \tfrac{1}{2})\lambda_{film}$$
$$m = 1, 2, 3, 4, \ldots$$

Now we can determine the optimum thickness of the film:

$$t_{min} = \frac{\lambda_{film}}{4} = \frac{\lambda_{vacuum}}{4n}$$

Where n is the refractive index of the film.

Now the optimum thickness for both PEDOT:PSS and ITO can be determined. After finding the optimum thicknesses of the two films under the incident wavelengths of 400, 500, 600, and 700nm, the data can be input into the simulation to find the reflectances. In *Figure 5 (a),* the reflectance under all incident wavelengths increases as the stack number increases. Generally, the rate of increase of reflectance decreases as the number of stacks rises. The

wavelength of the incident ray also correlates with the maximum reflectance. *Figure 5(b)* indicates that when the incident wavelength is 400nm, the reflectance approaches 0.887 as the stack number increases; when the incident wavelength is increased to 500nm, the reflectance drops by a little bit and approaches 0.878. As the incident ray wavelength increases to 600nm, there is a big drop in the maximum reflectance, which approaches 0.78. Lastly, when the incident wavelength is at 700nm, there is a considerable drop in maximum reflectance, approaching 0.56. The initial gradient of the hybrid TCF under an incident ray wavelength of 400nm is the largest when compared to the other three. Moreover, the curve also flattens the quickest among all four curves, suggesting that the maximum reflectance may be related to the initial gradient. Although the reflectance under 400nm incident wavelength is relatively high, it is nowhere near the desired reflectance of 0.99. This could be due to the nature of the simulation, in which the extinction coefficients are only 5 significant figures, which are much less precise than the original data.

(a) *(b)*

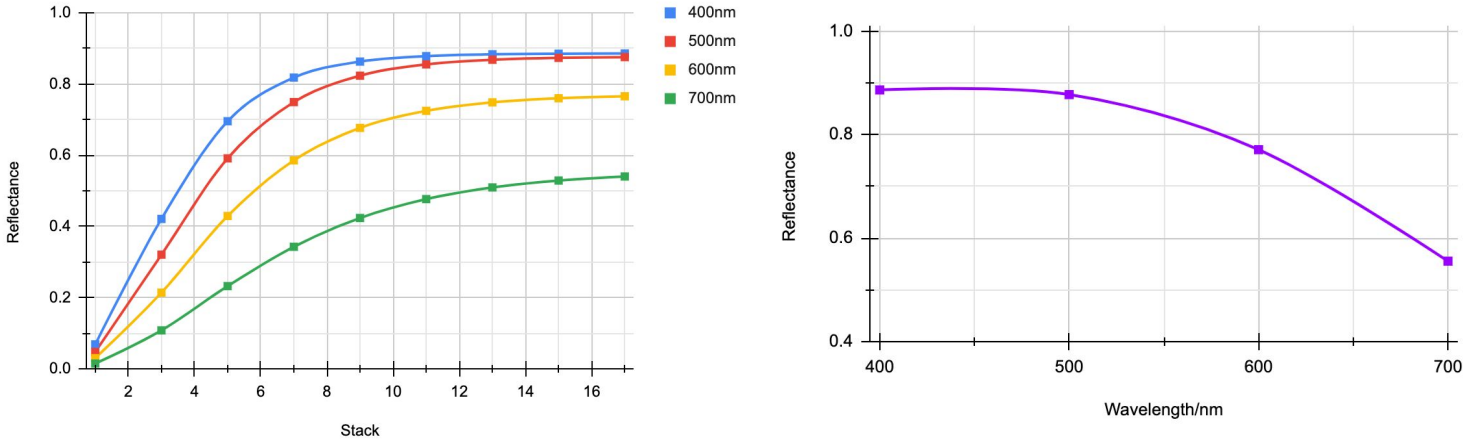

Figure 5 (a)*the reflectance for different stacks of hybrid TCFs under different incident ray wavelengths, where the thickness of each film is determined by* $t = \lambda_{vacuum}/4n$ ***(b)*** *the optimum reflectance for different hybrid TCFs under different incident ray wavelengths at 100 stacks, where the thickness of each film is determined by* $t = \lambda_{vacuum}/4n$

Discussion

The high reflectivity of the multiple stacks of PEDOT:PSS and ITO hybrid together with their good electrical conductivity ($1389\ S/cm$ for ITO[1] and $2\times10^{-4} S/cm$ to $2\times10^{-3} S/cm$ for PEDOT:PSS[12]) make them highly desirable in the laser industry, and they can be especially useful for making a Vertical-Cavity Surface-Emitting Laser (VCSEL). Unlike

conventional edge-emitting semiconductor lasers, VCSEL emits light in a cylindrical beam vertically out of the surface of a cylindrical wafer. VCSELs are widely used for many technologies such as fiber optics communications, facial recognition, and laser printing. VCSEL produces a circular light beam, which is very easy to couple into optical fibers. It also consumes less power compared to edge-emitting semiconductor lasers. VCSELs can also be integrated into a 2D array configuration. A VCSEL is composed of several layers; *figure 6(a)* demonstrates a simplified version of a VCSEL. The current is supplied to the structure through an electrical contact on the top layer. The next layer is a high reflectivity top Distributed Bragg Reflector (DBR) mirror. In the middle of the structure, there is the laser cavity. The two layers of oxides help to construct a light-emitting window to optimize the emitted light beam into a circular beam. Between the oxide layers, there is a quantum well layer where lazing happens. In the bottom, there is another DBR mirror with an even higher reflectance than the upper DBR mirror so that the lazing light will emit from the upper layer[13].

The hybrid transparent conducting films can be utilized to produce the DBR mirrors for a violet VCSEL, since the reflectance is the highest when the wavelength of the incident ray is at 400nm. In the hybrid TCF, PEDOT:PSS and ITO have different refractive indices, and by stacking the hybrid film, a DBR mirror can be obtained. The stack number can be altered to create a difference in reflectance between the upper and lower DBR mirrors. To illustrate, the upper layer can have 11 stacks, and the reflectance will be 0.878 and the bottom layer can be 15 stacks, with a corresponding reflectance of 0.885. The difference in reflectance between the two layers will be 0.007, which makes the lazing light travel through the surface of the structure.

(a) *(b)*

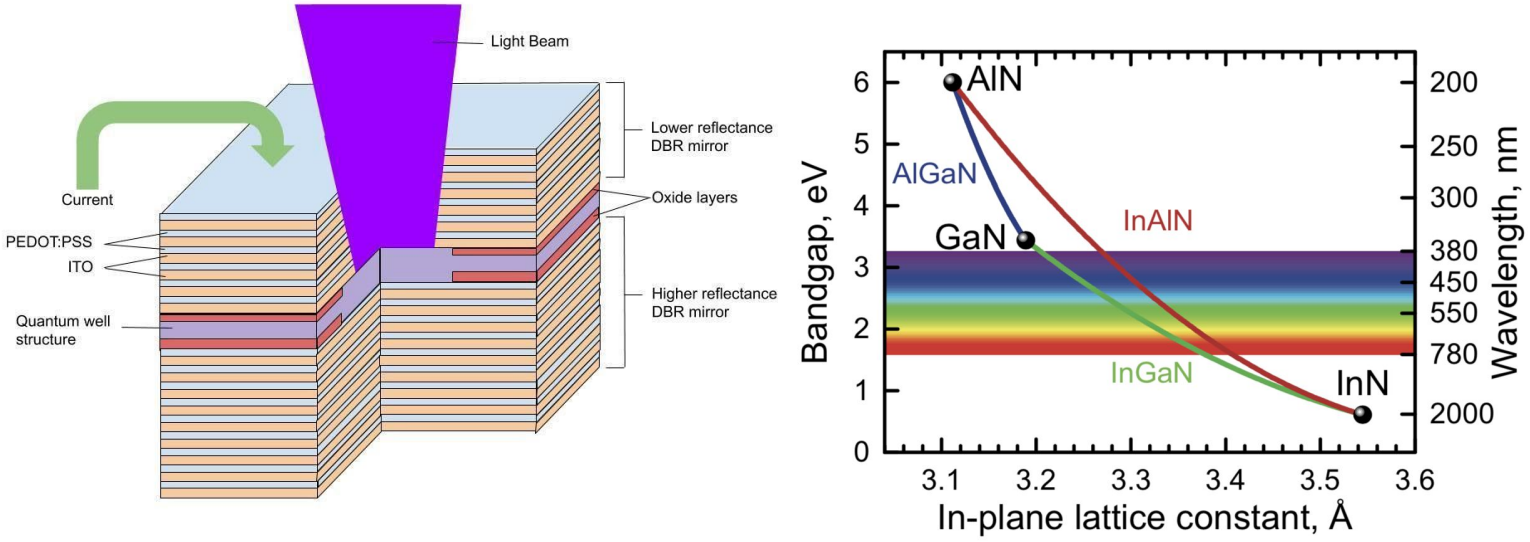

Figure 6 (a) *The simplified structure of a Vertical-Cavity Surface-Emitting Laser (VCSEL) produced with PEDOT:PSS and ITO hybrid stacks as the DBR mirrors.* ***(b)*** *Bandgaps of wurtzite GaN, AlN, and InN and their alloys versus their lattice constant at 300 K, from D S Arteev et al 2018 J. Phys.: Conf. Ser.* ***1135*** *012050*

The active layer of the structure should emit lazing light of wavelength equal to 400nm since it is where the hybrid film has the optimal reflectance. In the active layer, a quantum well structure is utilized to produce a lazing of the desired wavelength. InGaN and AlGaN are suitable materials for the active layer. In *Figure 6(b)*[14], GaN has a band gap energy of around 3.4 eV and a corresponding wavelength of around 370 nm. InN has a corresponding band gap wavelength of around 2000nm. A certain ratio of InN and GaN can be used to produce the alloy InGaN so that its corresponding band gap wavelength will be 400nm. The AlGaN alloy has a higher band gap energy than the InGaN alloy; hence, can be used to create a quantum well. When the lazing light is emitted, it will reflect between the two DBR mirrors and a violet laser will emit from the surface of the structure.

Evaluation

The data has a number of limitations, for example, the simulation limits the number of significant figures that could be entered, which caused systematic errors. Moreover, the gap between the wavelengths selected were too large to observe a clear trend, and the curves demonstrated on the graphs were all based on the existing data points. Moreover, since all the experiments were conducted on computer simulations, the next research step would be to conduct actual experiments to validate the results of the simulation.

Conclusion

The "PhotonicsRT: Wave Propagation In Multilayer Structures" simulation showed that for a single stack, the absorption of a combination of PEDOT:PSS and ITO film may be affected by the ratio of thickness and the wavelength of the incident light. This relationship is related to the extinction coefficient of the two materials, as an intersection of the curves is also observed when the incident ray wavelength is around 480nm. The study shows that for multiple stacks with optimum thickness ratio of each film, the reflectance increases as the stack number increases. Moreover, the reflectance increases as the incident ray wavelength decreases in the visible spectrum. When the incident wavelength is 400nm, the reflectance is the largest, saturating at around 0.9. The stack dependent nature of this structure can be utilized to make DBR mirrors used in a VCSEL to produce violet lasers.

Acknowledgments

The author would like to acknowledge his classmate from the Pioneer Academics program who gave him valuable suggestions. The author gratefully acknowledges Professor F. Peiris who helped him edit the paper and guided him to finish his first research paper. The author also acknowledges Pioneer Academics for providing him with access to the Oberlin online library as well as the writing center.

References

[1] Chen, Zhangxian, et al. "Fabrication of Highly Transparent and Conductive Indium–Tin Oxide Thin Films with a High Figure of Merit via Solution Processing." *Langmuir*, vol. 29, no. 45, 2013, pp. 13836–13842., doi:10.1021/la4033282.

[2] Contreras, Miguel A., et al. "Replacement of Transparent Conductive Oxides by Single-Wall Carbon Nanotubes in Cu(In,Ga)Se2-Based Solar Cells." *The Journal of Physical Chemistry C*, vol. 111, no. 38, 2007, pp. 14045–14048., doi:10.1021/jp075507b.

[3] Ginley, David S., and John D. Perkins. "Transparent Conductors." *Handbook of Transparent Conductors*, 2010, pp. 1–25., doi:10.1007/978-1-4419-1638-9_1.

[4] Niu, Chunming. “Carbon Nanotube Transparent Conducting Films.” *Fundamentals of Materials for Energy and Environmental Sustainability*, by D. S. Ginley and David Kahen, Cambridge University Press, 2012, pp. 766–772.

[5] Solar Power Europe. *Global Market Outlook For Solar Power / 2018 - 2022*, Solar Power Europe, 2017.

[6] Stadler, Andreas. “Transparent Conducting Oxides—An Up-To-Date Overview.” *Materials*, vol. 5, no. 12, 2012, pp. 661–683., doi:10.3390/ma5040661.

[7] Wang, Yang, and George J. Weng. “Electrical Conductivity of Carbon Nanotube- and Graphene-Based Nanocomposites.” *Micromechanics and Nanomechanics of Composite Solids*, 2017, pp. 123–156., doi:10.1007/978-3-319-52794-9_4.

[8] Satoshi Ishii, Uday K. Chettiar, Xingjie Ni, Alexander V. Kildishev (2014), "PhotonicsRT: Wave Propagation in Multilayer Structures," https://nanohub.org/resources/photonicsrt. (DOI: 10.4231/D3MK6588C).

[9] M. N. Polyanskiy, "Refractive index database," https://refractiveindex.info. Accessed on 2020-08-23.

[10] Byrnes, Steven J. “Multilayer Optical Calculations.” *ArXiv*, 18 Nov. 2019, arxiv.org/abs/1603.02720v4.

[11]Duffy, Andrew. *Diffraction; Thin-Film Interference*, 2007, physics.bu.edu/~duffy/py106/Diffraction.html.

[12] Yu, Zhimeng, et al. “PEDOT:PSS Films with Metallic Conductivity through a Treatment with Common Organic Solutions of Organic Salts and Their Application as a Transparent Electrode of Polymer Solar Cells.” *ACS Applied Materials & Interfaces*, vol. 8, no. 18, 2016, pp. 11629–11638., doi:10.1021/acsami.6b00317.

[13] Kuramoto, Masaru, et al. “Watt-Class Blue Vertical-Cavity Surface-Emitting Laser Arrays.” *Applied Physics Express*, vol. 12, no. 9, 2019, p. 091004., doi:10.7567/1882-0786/ab3aa6.

[14] Arteev, D S, et al. “Investigation of Statistical Broadening in InGaN Alloys.” *Journal of Physics: Conference Series*, vol. 1135, 2018, p. 012050., doi:10.1088/1742-6596/1135/1/012050.